PNAS RESEARCH ARTICLE | NEUROSCIENCE

Enhancement of the liver's neuroprotective role ameliorates traumatic brain injury pathology

Yongfeng Dai[a,b,1], Jinghua Dong[a,b,1], Yu Wu[b,c], Minzhen Zhu[b], Wenchao Xiong[a], Huanyu Li[b], Yulu Zhao[a,b], Bruce D. Hammock[d,e,2], and Xinhong Zhu[a,b,c,f,2]

Contributed by Bruce D. Hammock; received January 26, 2023; accepted May 19, 2023; reviewed by Fernando Gomez-Pinilla, Andrew A. Pieper, and Naomi Sayre

Traumatic brain injury (TBI) is a pervasive problem worldwide for which no effective treatment is currently available. Although most studies have focused on the pathology of the injured brain, we have noted that the liver plays an important role in TBI. Using two mouse models of TBI, we found that the enzymatic activity of hepatic soluble epoxide hydrolase (sEH) was rapidly decreased and then returned to normal levels following TBI, whereas such changes were not observed in the kidney, heart, spleen, or lung. Interestingly, genetic downregulation of hepatic *Ephx2* (which encodes sEH) ameliorates TBI-induced neurological deficits and promotes neurological function recovery, whereas overexpression of hepatic sEH exacerbates TBI-associated neurological impairments. Furthermore, hepatic sEH ablation was found to promote the generation of A2 phenotype astrocytes and facilitate the production of various neuroprotective factors associated with astrocytes following TBI. We also observed an inverted V-shaped alteration in the plasma levels of four EET (epoxyeicosatrienoic acid) isoforms (5,6-, 8,9-,11,12-, and 14,15-EET) following TBI which were negatively correlated with hepatic sEH activity. However, hepatic sEH manipulation bidirectionally regulates the plasma levels of 14,15-EET, which rapidly crosses the blood–brain barrier. Additionally, we found that the application of 14,15-EET mimicked the neuroprotective effect of hepatic sEH ablation, while 14,15-epoxyeicosa-5(Z)-enoic acid blocked this effect, indicating that the increased plasma levels of 14,15-EET mediated the neuroprotective effect observed after hepatic sEH ablation. These results highlight the neuroprotective role of the liver in TBI and suggest that targeting hepatic EET signaling could represent a promising therapeutic strategy for treating TBI.

traumatic brain injury | liver | soluble epoxide hydrolase | 14,15-epoxyeicosatrienoic acid | astrocytes

Significance

To date, no effective treatments are available for traumatic brain injury (TBI). Here, we identified the neuroprotective role of the liver in TBI. Hepatic sEH (soluble epoxide hydrolase) activity was specifically altered following TBI and negatively correlated with the plasma levels of 14,15-EET (-epoxyeicosatrienoic acid). Hepatic sEH manipulation bidirectionally modulated TBI-induced neurological deficits by regulating the generation of A2 phenotype astrocytes. Peripheral 14,15-EET rapidly crossed the blood–brain barrier. Moreover, 14,15-EET mimicked the neuroprotective effects of hepatic *Ephx2* deletion, whereas 14,15-epoxyeicosa-5(Z)-enoic acid blocked the neuroprotective effects of hepatic sEH ablation following TBI. These results highlight the neuroprotective role of the liver in TBI and suggest that targeting this neuroprotective role may represent a promising therapeutic strategy for TBI.

Traumatic brain injury (TBI) is a major cause of morbidity and mortality worldwide (1, 2). Neuroprotective therapies aimed at relieving TBI-induced damage by reducing glutamate toxicity, mitochondrial dysfunction, and inflammation have attracted increasing attention over the past few decades (2–4). However, to date, the translation of preclinical research findings on neuroprotection into clinical practice has been unsuccessful because of the complexity and heterogeneity of TBI (5, 6). Accordingly, single-target drugs are unlikely to be effective and it may be beneficial to identify drugs with multiple mechanisms of action, or combinations of drugs with independent but complementary mechanisms of action (2, 7). With this in mind, the lack of attention to peripheral organs is somewhat surprising given their unique biological and anatomical properties that support brain function.

Recent studies have shown that peripheral organs play an important role in maintaining normal central nervous system function. For example, a specific gut microbiome has been associated with short-term memory, working memory, and volume of the hippocampus and frontal regions of the brain (8). In another study, hepatic soluble epoxide hydrolase (sEH) (encoded by *EPHX2*) regulated the behavioral and cellular effects of chronic stress (9). Increasing evidence indicates that TBI affects not only the brain, but also the liver, heart, lungs, gut, and immune system (6, 10, 11). However, the contribution of the peripheral organs to TBI remains unclear.

We proposed that the liver plays a prominent role in the pathophysiology of TBI. The liver is the largest organ in the body and produces a wide range of biochemical factors necessary for brain function (12). Clinical studies have reported that the overall mortality in patients with TBI and cirrhosis is nearly twice that in patients without cirrhosis (13). Blood stasis in hepatic sinus capillaries and veins, as well as erythrocyte adherence to blood vessel walls, has been observed in a rat model of TBI (14). Evidence has shown that polyunsaturated fatty acids (PUFAs) effectively ameliorate TBI-induced neurobehavioral outcomes (15). The brain is highly enriched in PUFAs, particularly arachidonic acid, but

Reviewers: F.G.-P., University of California Los Angeles; A.A.P., Case Western Reserve University; and N.S., The University of Texas Health Science Center at San Antonio.

The authors declare no competing interest.

[1]Y.D. and J.D. contributed equally to this work.

[2]To whom correspondence may be addressed. Email: bdhammock@ucdavis.edu or zhuxh527@126.com.

This article contains supporting information online at https://www.pnas.org/lookup/suppl/doi:10.1073/pnas.2301360120/-/DCSupplemental.

Published June 20, 2023.

only takes up PUFAs from the plasma following de novo synthesis in the liver (9, 16). Finally, 14,15-epoxyeicosatrienoic acid (-EET) is a downstream product of PUFA metabolism, which has neuroprotective effects in a variety of diseases (9, 17) and can be metabolized by sEH to the far less active and more polar 14,15-dihydroxyeicosatrienoic acid (-DHET) (18). Studies have shown that the genetic deletion of *Ephx2* or pharmacological inhibition of sEH ameliorates the pathology in mice (19–21). Notably, sEH is widely expressed in peripheral organs, especially in the liver (22). In this study, we investigated whether hepatic EET signaling is involved in the pathophysiology of TBI and aimed to understand the underlying mechanisms.

Results

Hepatic sEH Activity Was Specifically Altered Following TBI. The controlled cortical injury (CCI) is a well-established model of TBI in mice and has the advantages of stability, ease of operation, and high repeatability (23). To investigate the role of peripheral organs in the pathophysiology of TBI, we characterized changes in the enzymatic activity of sEH in peripheral organs following CCI. We found that hepatic sEH activity was significantly decreased 0.5 to 3 h after CCI, and returned to normal levels 24 h after CCI, presenting a "V"-shape change (Fig. 1*A*). In contrast, no significant change in sEH activity was observed in other peripheral organs including the kidney, heart, spleen, and lung. However, no significant changes were observed in the mRNA and protein levels of hepatic sEH at any time point (Fig. 1 *B* and *C*). In addition, we found that the enzymatic activity of sEH in the injured cortex did not show significant changes, while the protein levels of sEH increased at 3 h and 24 h after CCI (Fig. 1 *A* and *D*). These results indicated that hepatic sEH activity was temporally and specifically altered following CCI.

The closed head injury (CHI) model is a clinically relevant model of TBI (24). To further investigate the role of the liver in TBI, we therefore detected whether hepatic sEH activity was altered following CHI and found that hepatic sEH activity was specifically decreased at 1 h after CHI, then returned to normal levels 3 h after CHI, also resembling a "V"-shape change. No significant changes were observed in the kidney, heart, spleen, lung, or injured cortex (Fig. 1*E*). We also found that the protein levels of hepatic sEH were not altered, and sEH expression increased in the injured cortex 3 h after CHI (Fig. 1*F*). Taken together, these results strongly indicate that hepatic sEH activity plays a role in the pathophysiology of TBI.

Downregulation of Hepatic sEH Ameliorated CCI-Induced Neurological Deficits. To determine the role of hepatic sEH in the pathology, we specifically knocked down *Ephx2* in the liver via tail vein injection of recombinant adeno-associated

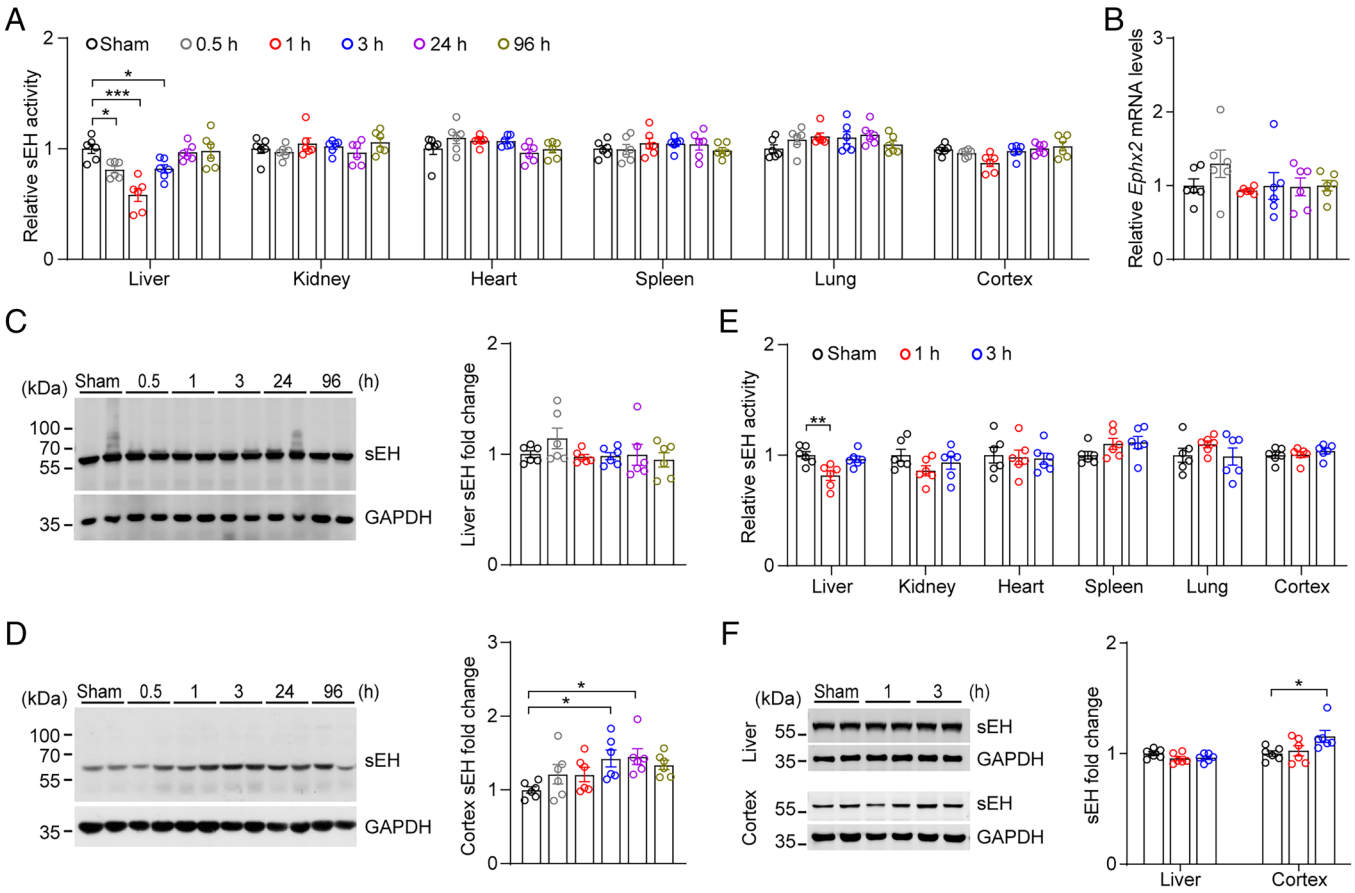

Fig. 1. Enzymatic activity of sEH was specifically altered in the liver following TBI. (*A*) Relative sEH activity in the liver, kidney, heart, spleen, lung, and injured cortex was examined at different time points following CCI in adult male C57BL/6J mice ($n = 6$). (*B*) The relative mRNA levels of *Ephx2* in the liver at different time points after CCI. (*C* and *D*) Western blotting (*Left*) and quantification (*Right*) of sEH in the liver (*C*), and injured cortex (*D*), at different time points after CCI ($n = 6$). (*E*) Relative sEH activity of the liver, kidney, heart, spleen, lung, and injured cortex at different time points following CHI in adult male C57BL/6J mice ($n = 6$). (*F*) Western blotting (*Left*) and quantification (*Right*) of sEH in the liver and injured cortex at different time points after CHI ($n = 6$). Statistical significance was determined using one-way ANOVA with the Dunnett's post-hoc test or Brown–Forsythe and Welch ANOVA followed by the Dunnett's T3 post-hoc test. Data are presented as the means ± SEM. Asterisks indicate significant differences (*$P < 0.05$, **$P < 0.01$, ***$P < 0.001$).

virus (rAAV) 2/8-eGFP-*Ephx2*-shRNA into adult C57BL/6J mice (Fig. 2*A*). Histological studies showed that eGFP+ cells were observed only in the liver but not in the kidney, heart, spleen, or lung 2 wk after virus injection (*SI Appendix,* Fig. S1*A*). rAAV2/8-eGFP-*Ephx2*-shRNA injection significantly decreased both the protein levels and activity of hepatic sEH and had no effect on sEH activity in other peripheral organs compared to mice injected with rAAV2/8-eGFP-scrambled (SC)-shRNA (*SI Appendix,* Fig. S1 *B* and *C*), validating the viral approach (9). All mice were subjected to CCI, except for the sham animals, in which a craniotomy was performed and the dura was exposed without impact. Interestingly, knockdown of hepatic sEH significantly decreased brain lesion volume and the lesion/total volume ratio following CCI compared to CCI mice injected with rAAV2/8-eGFP-SC-shRNA (Fig. 2 *B* and *C* and *SI Appendix,* Fig. S1*D*).

TBI is a devastating injury that often results in long-term neurological deficits, including locomotor function and memory impairments (25, 26). We then assessed the effect of hepatic *Ephx2* knockdown on CCI-induced neurological deficits using behavioral tests. Two days after CCI, mice were subjected in the open field test (OFT), and we found that mice injected with rAAV2/8-eGFP-SC-shRNA walked shorter distances than those of sham animals injected with rAAV2/8-eGFP-SC-shRNA (Fig. 2*D*). This result is consistent with a previous study (27). Intriguingly, the rAAV2/8-eGFP-*Ephx2*-shRNA injection reversed the locomotor deficits induced by CCI. To evaluate sensorimotor function, we performed a rotarod performance test on day 1 and 3 post-CCI and found that CCI induced motor coordination deficits compared to sham mice injected with rAAV2/8-eGFP-SC-shRNA. In contrast, mice injected with rAAV2/8-eGFP-*Ephx2*-shRNA showed significantly improved performance in the rotarod test following CCI compared to CCI mice injected with rAAV2/8-eGFP-SC-shRNA (Fig. 2*E*). Moreover, in the Y-maze task, knockdown of hepatic sEH reversed the decrease in the percentage of alternations induced by CCI (Fig. 2*F*). Together, these results suggest that the downregulation of hepatic sEH and the expected increase in epoxy-fatty acids (EpFAs) ameliorated the pathology of CCI.

Next, we examined whether overexpression of hepatic sEH aggravated CCI-induced neurological impairment. Adult C57BL/6J mice were tail vein-injected with rAAV2/8-eYFP-*Ephx2* or control virus rAAV2/8-eYFP (*SI Appendix,* Fig. S1*E*). Again, we found that eYFP-positive cells were only observed in the liver 4 wk after viral

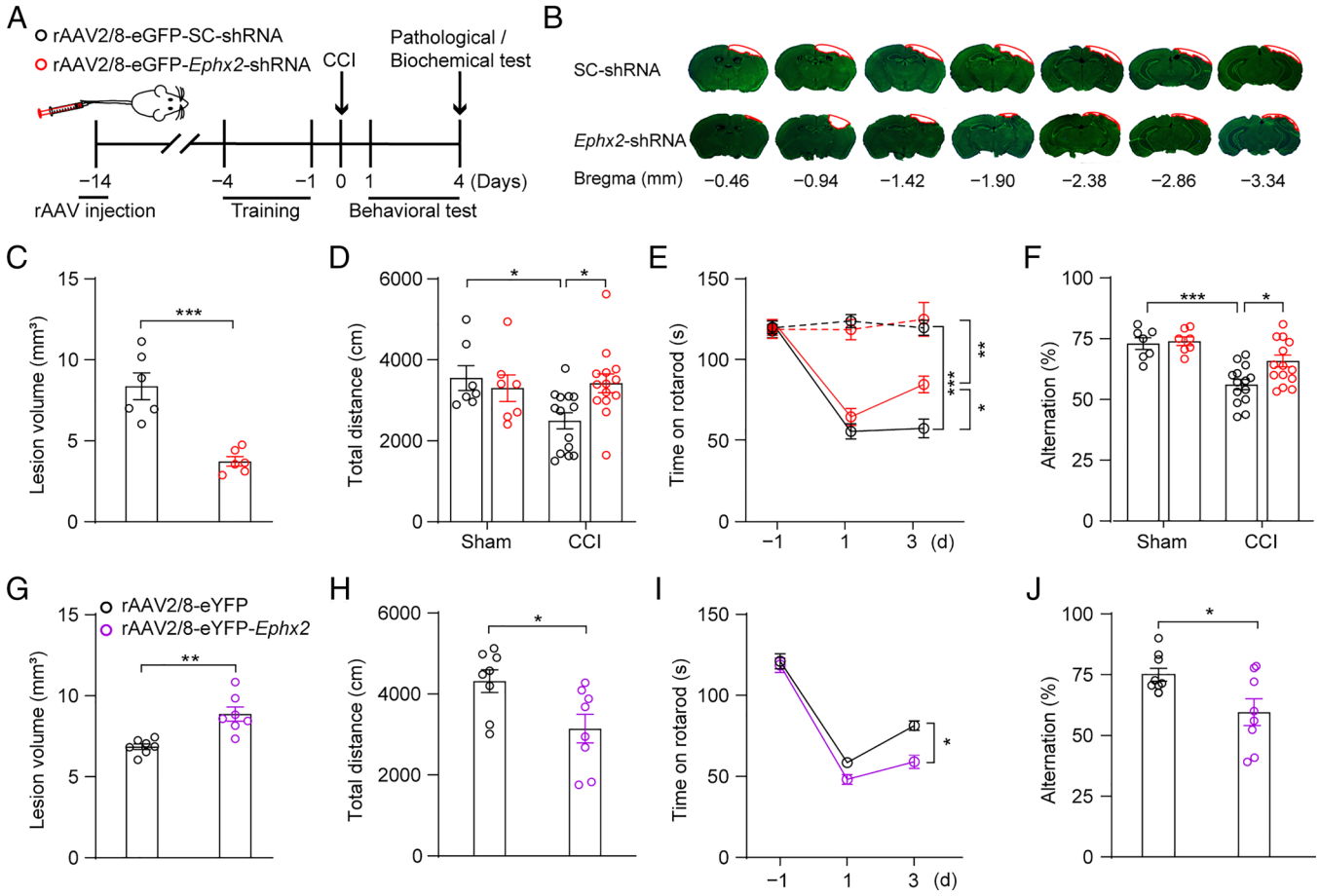

Fig. 2. Manipulation of hepatic sEH using tail vein-virus injection modulated CCI-induced neurological deficits. (*A*) Schematic diagram of the experimental design. Black circles, control animals; red circles, adult C57BL/6J mice injected with rAAV2/8-eGFP-*Ephx2*-shRNA. (*B–F*) The effects of knocking-down hepatic *Ephx2* following CCI. (*B*) Representative images of Nissl staining for brain injury. The red outline showing the loss area of injured brain. (*C*) Quantitative analysis of brain lesion volume (n = 6). (*D*) Spontaneous locomotor activity was assessed using the OFT (sham, n = 7; CCI, n = 14). (*E*) Sensorimotor function was assessed using the rotarod performance test at 1 d pre-CCI and 1, 3 d post-CCI (dashed line for sham group, n = 7; and solid line for CCI group, n = 14). (*F*) Spatial memory ability was tested using the Y-maze test (sham, n = 7; CCI, n = 14). (*G–J*) The effects of overexpression of *Ephx2* in the liver in CCI. Black circles, control animals; purple circles, adult C57BL/6J mice injected with rAAV2/8-eYFP-*Ephx2*. (*G*) Quantitative analysis of brain lesion volume (n = 7). (*H*) OFT, (*I*) rotarod performance test, and (*J*) Y-maze test in rAAV2/8 virus-injected mice after CCI (n = 8). Statistical significance was determined using two-tailed unpaired Student's t test for *C*, *G*, *H*, and *J*; two-way ANOVA followed by the Bonferroni's post hoc-test for *D* and *F*; or two-way repeated measures ANOVA followed by the Bonferroni's post hoc-test for *E* and *I*. Data are presented as the means ± SEM. Asterisks indicate significant differences (*P < 0.05, **P < 0.01, ***P < 0.001).

injection (*SI Appendix,* Fig. S1*F*). As expected, hepatic sEH protein levels and activity were significantly increased in mice injected with rAAV2/8-eYFP-*Ephx2* compared to control animals, whereas hepatic sEH overexpression had little effect on sEH activity in other peripheral organs (*SI Appendix,* Fig. S1 *G* and *H*). Notably, the lesion volume in mice injected with rAAV2/8-eYFP-*Ephx2* was significantly larger than that in CCI mice injected with rAAV2/8-eYFP (Fig. 2*G* and *SI Appendix,* Fig. S1 *I* and *J*). Neurological function assessments showed that the CCI mice injected with rAAV2/8-eYFP-*Ephx2* traveled a shorter distance in the OFT, spent less time on the rotarod, and had a lower percentage of alternations in the Y-maze test (Fig. 2 *H–J*) than that of the CCI mice injected with rAAV2/8-eYFP. Taken together, these results indicate that hepatic sEH plays an essential role in the pathology of TBI.

Hepatic *Ephx2* Deletion Produced Neuroprotective Effect and Promoted the Generation of A2 Astrocytes in the Injured Cortex. To further characterize the role of hepatic sEH in the pathophysiology of TBI, we performed experiments using *Albumin*-creER^{T2}; *Ephx2*$^{loxp/loxp}$ double-transgenic mice, in which hepatic sEH was deleted following a 5-d tamoxifen (TAM) injection (henceforward referred to as cKO mice) (Fig. 3*A* and *SI Appendix,* Fig. S2*A*). Adult littermate *Ephx2*$^{loxp/loxp}$ mice with normal sEH protein levels in the liver after TAM injection served as wild-type (WT) controls. Hepatic sEH activity in cKO mice was significantly decreased compared to that in WT mice, whereas sEH activity in other peripheral organs was unaffected by hepatic sEH ablation (*SI Appendix,* Fig. S2*B*). We found that hepatic sEH ablation significantly decreased the lesion volume in

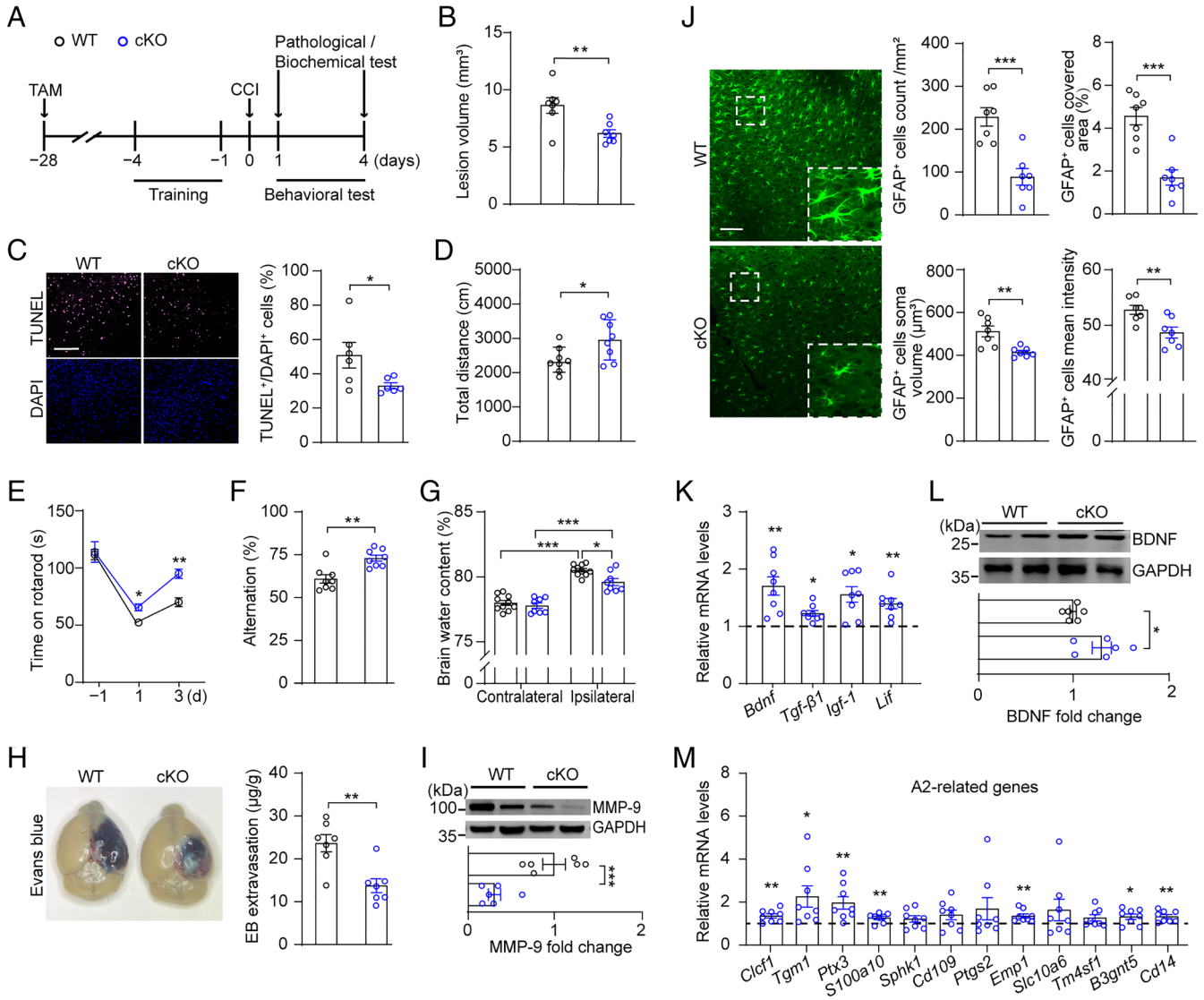

Fig. 3. Hepatic sEH ablation ameliorated CCI-induced neurological deficits. (*A*) Schematic diagram of the experimental design. TAM, tamoxifen; Black circles, WT; blue circles, cKO. (*B*) Quantitative analysis of brain lesion volume (n = 7). (*C*, *Left*) representative TUNEL (purple) and DAPI-stained (blue) brain slices of WT and cKO mice at 1 d post-CCI; (*C*, *Right*) quantification analysis percentage of TUNEL-positive cells (n = 6). (Scale bar: 100 μm.) (*D*) OFT, (*E*) rotarod performance test, and (*F*) Y-maze test in WT and cKO mice after CCI (n = 8). (*G*) The water content in the ipsilateral and contralateral brain (WT, n = 10; cKO, n = 8). (*H*) Quantitation of Evans blue extravasation in brain at 4 d post-CCI (n = 7). (*I*) Western blotting and quantification of cortex MMP-9 at 4 d post-CCI (n = 6). (*J*) Representative images (*Left*) of GFAP+ astrocytes in the injured cortex, and the proportion of covered area, number, soma volume, and mean intensity of GFAP+ astrocytes were quantitatively analyzed (n = 7). (Scale bar: 100 μm.) (*K*) Relative mRNA levels of neuroprotective factors related to astrocyte's function in the injured cortex (dashed line indicates the mean levels of each corresponding gene in WT controls, n = 8). (*L*) Western blotting and quantification of cortex BDNF at 4 d post-CCI (n = 6). (*M*) Relative mRNA levels of genes associated with A2 phenotype astrocytes in the injured cortex (dashed line indicates the mean levels of each corresponding gene in WT controls, n = 8). Statistical significance was determined using two-tailed unpaired Student's t test for *B–D*, *F*, *H–J*, and *L*; two-way repeated-measures ANOVA followed by the Bonferroni's post-hoc test for *E*; two-way ANOVA followed by the Bonferroni's post-hoc test for *G*; or multiple t tests for *K* and *M*. Data are presented as the means ± SEM. Asterisks indicate significant differences (*P < 0.05, **P < 0.01, ***P < 0.001).

the brain 4 d after CCI compared to that in WT mice (Fig. 3*B* and *SI Appendix*, Fig. S2 *C* and *D*). To investigate the effect of hepatic sEH ablation on cell death, we performed terminal deoxynucleotidyl transferase dUTP nick end labeling (TUNEL) staining (28). No TUNEL+ cells were detected in the brain slices of sham animals (*SI Appendix*, Fig. S2*E*). In contrast, numerous TUNEL+ cells were observed in the brain slices of WT mice 1 d after CCI. Intriguingly, hepatic sEH ablation significantly decreased the number of TUNEL+ cells in the injured cortex compared to that in CCI-WT mice (Fig. 3*C*). Behavioral analysis showed that, compared with CCI-WT animals, CCI-cKO mice exhibited significantly better postinjury performance in the OFT, rotarod test, and Y-maze test (Fig. 3 *D*–*F*). These results clearly showed that hepatic sEH ablation produced a neuroprotective effect in the CCI mouse model.

Blood–brain barrier (BBB) disruption is a hallmark feature of TBI and is associated with brain edema and neuronal death (29). Studies have shown that sEH inhibitors protect the BBB from brain injury (30–32). Therefore, we investigated whether deletion of hepatic *Ephx2* protected the BBB following CCI. We first measured the brain water content in the injured (ipsilateral) and uninjured (contralateral) cortex 24 h after CCI and found that CCI led to a significant increase in brain water content in the ipsilateral cortex of WT mice compared to that in the contralateral cortex (Fig. 3*G*). In contrast, hepatic sEH ablation significantly decreased the brain water content in the ipsilateral cortex compared to that in WT mice, although this content was still higher than that of the contralateral cortex in cKO mice. We then used the Evans blue extravasation to assess BBB integrity (33). We observed a weak blue dye in the brains of sham animals. However, CCI induced BBB breakdown, showing a heavy blue dye in the brains of WT mice. In contrast, hepatic sEH ablation significantly reduced BBB permeability following CCI (Fig. 3*H* and *SI Appendix*, Fig. S2*F*). Moreover, we found that the protein levels of matrix metalloproteinase (MMP)-9, which disrupts the BBB by degrading tight junction proteins and the basal lamina (34), were increased in the injured cortex of WT mice compared to those of sham controls, whereas hepatic sEH ablation significantly decreased MMP-9 expression 4 d after CCI compared to CCI-WT mice (Fig. 3*I* and *SI Appendix*, Fig. S2*G*). These results suggested that hepatic sEH ablation reduced BBB permeability in CCI mice.

Astrocytes respond to TBI through altered gene expression, hypertrophy, and proliferation (35, 36). To further characterize the mechanisms underlying hepatic neuroprotection, we examined the effects of hepatic sEH ablation on the astrocyte number and morphology. Immunostaining showed that the covered area, number, soma volume, and mean intensity of GFAP+ astrocytes in the injured cortex of cKO mice were significantly lower than those in WT mice (Fig. 3*J*). We then examined the genes of neuroprotective factors and cytokines associated with astrocytes and found that the mRNA levels of *Bdnf* (encodes brain-derived neurotrophic factor, BDNF), *Tgf-β1* (encodes transforming growth factor-beta 1), *Igf-1* (encodes insulin-like growth factor 1), and *Lif* (encodes leukemia inhibitory factor) were significantly increased in the injured cortex of cKO mice compared with that in WT animals following CCI (Fig. 3*K*). Moreover, western blotting showed that the protein levels of BDNF were increased in the injured cortex of CCI-cKO mice compared to those in CCI-WT animals (Fig. 3*L* and *SI Appendix*, Fig. S2*G*). These results indicated that reactive astrocytes may be involved in the neuroprotective effects of hepatic sEH ablation.

Reactive astrocytes differ significantly in their core gene expression and functions, named A1 and A2, respectively, with A1 showing detrimental effects and A2 being neuroprotective (37). Moreover, *LIF* is greatly induced in stroke-reactive astrocytes (A2 astrocytes) but only marginally induced in lipopolysaccharide (LPS)-induced reactive astrocytes (A1 astrocytes) (38). Therefore, we predicted that hepatic sEH ablation would promote the generation of A2 phenotype–reactive astrocytes. To test this hypothesis, we examined the mRNA levels of genes related to A1 and A2 phenotype astrocytes and found that the levels of 1 of the 12 A1-related genes were decreased in the injured cortex of cKO mice compared with those of WT controls following CCI (*SI Appendix*, Fig. S2*H*). In contrast, for A2-related genes in the injured cortex, the mRNA levels of 7 of the 12 genes were significantly up-regulated in cKO mice relative to those in WT mice (Fig. 3*M*). In addition, no significant differences were observed in the covered area, number, or volume of Iba-1+ microglia between the WT and cKO mice after CCI, although the mean intensity of Iba-1+ microglia was marginally affected by hepatic sEH ablation (*SI Appendix*, Fig. S2*I*). Moreover, most genes associated with the phagocytic function of microglia did not differ between the two groups, except for *Bst2* (*SI Appendix*, Fig. S2*J*). Therefore, these results suggest that the observed neuroprotective effects of hepatic *Ephx2* deletion following CCI may be due to the promotion of A2 phenotype–reactive astrocytes.

Hepatic sEH Activity Specifically Modulated the Plasma Levels of 14,15-EET. sEH hydrolyzes EpFAs including EETs, linoleic acid, and ω-3 lipids. Among the EpFAs, EETs have exceptionally high biological activity, making them attractive for therapeutic applications (39). Alternatively, EETs are metabolized via a variety of pathways; sEH, which hydrolyzes EETs into DHETs, is the dominant pathway in many tissues (40). Our previous study indicates that hepatic sEH is involved in the regulation of plasma EETs, especially 14,15-EET (9). To investigate the mechanisms underlying hepatic neuroprotection, we measured plasma levels of EETs following TBI. We found that the plasma levels of EETs, including 5,6-, 8,9-, 11,12-, and 14,15-EET, were increased 1 h and 3 h after CCI, and returned to the normal levels 24 h after CCI, representing an inverted "V"-shape change (Fig. 4*A* and *SI Appendix*, Fig. S3*A*). A negative correlation was observed between hepatic sEH activity and plasma EETs levels (Fig. 4*B* and *SI Appendix*, Fig. S3 *B*–*D*). A change in the ratio of epoxides to their corresponding diols in the plasma could be an indicator of hepatic sEH activity (9). We therefore calculated the ratios of plasma DHETs/EETs and found that the ratio of 14,15-DHET/EET resembled a "V"-shape change (*SI Appendix*, Fig. S3*E*), further supporting the notion that hepatic sEH activity temporally decreases after CCI. However, in the CHI model, we found that only the plasma levels of 14,15-EET increased 1 h after CHI and returned to normal 3 h after CHI. No significant changes were observed in the plasma levels of the other three EET isoforms (Fig. 4*C* and *SI Appendix*, Fig. S3*G*). We observed a negative correlation between hepatic sEH activity and plasma 14,15-EET levels following CHI (Fig. 4*D*). Moreover, we found that the ratio of 14,15-DHET/EET in the CHI model also resembled a "V"-shape change (*SI Appendix*, Fig. S3*H*). In addition, the concentration of 14,15-EET in the injured cortex did not show significant changes in two mouse models of TBI (*SI Appendix*, Fig. S3 *F* and *I*). Intriguingly, genetic manipulation of hepatic sEH bidirectionally and specifically regulated the plasma levels of 14,15-EET (Fig. 4 *E*–*G* and *SI Appendix*, Fig. S4), and the plasma level of 14,15-EET negatively correlated with hepatic sEH activity in these animals 4 d after CCI (Fig. 4*H*). These results indicate that hepatic sEH specifically regulates plasma levels of 14,15-EET.

Next, we determined whether 14,15-EET crossed the BBB. To this end, deuterium-labeled 14,15-EET (14,15-EET-d_{11}), a tracer of 14,15-EET, was injected into the carotidal artery of adult C57BL/6J mice pretreated with a sEH inhibitor

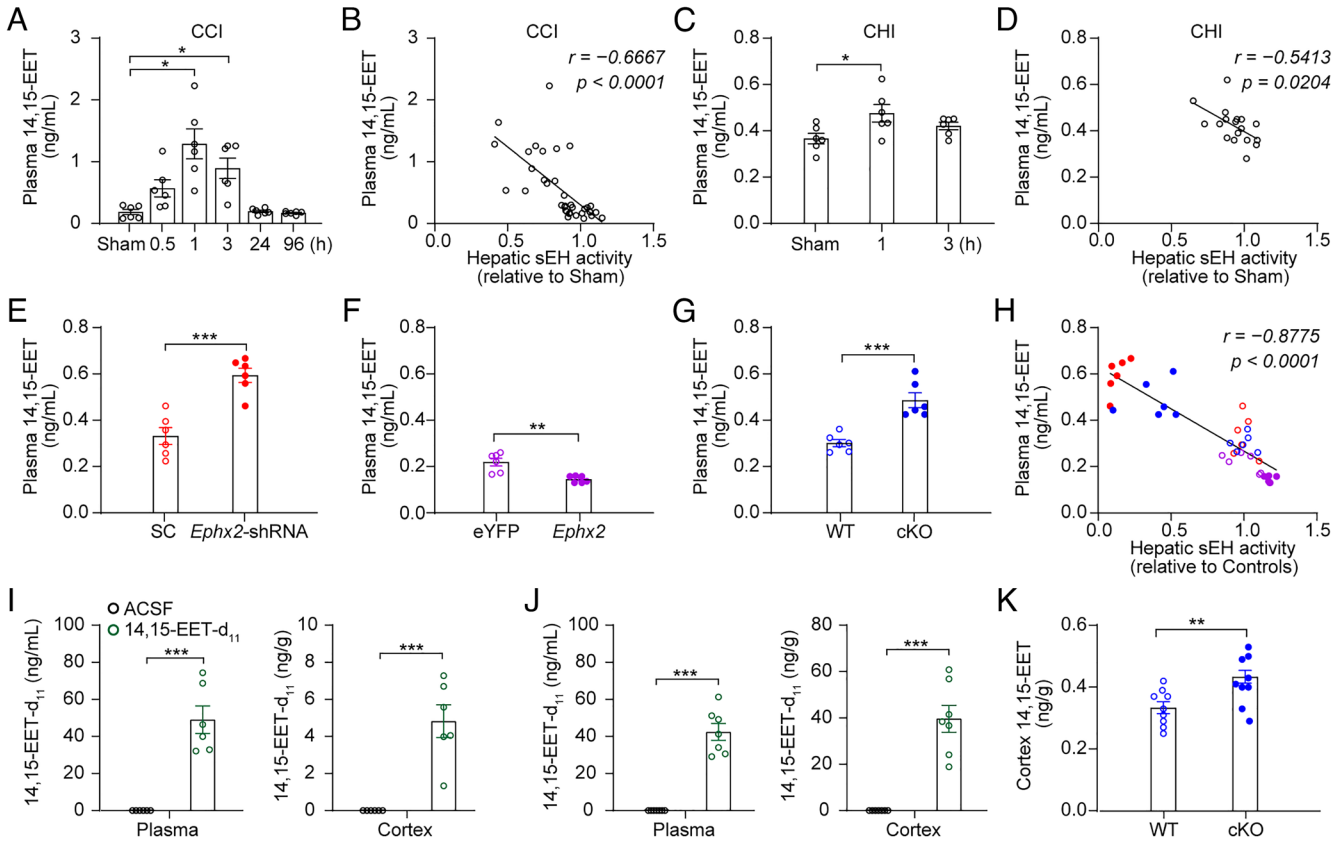

Fig. 4. Hepatic sEH activity specifically modulated the plasma levels of 14,15-EET. (*A*) The plasma levels of 14,15-EET at different time points post-CCI in adult male C57BL/6J mice (n = 6 per time point). (*B*) Negative correlation was found between hepatic sEH activity and plasma 14,15-EET levels following CCI. (*C*) The plasma levels of 14,15-EET at different time points post-CHI in adult male C57BL/6J mice (n = 6 per time point). (*D*) Negative correlation was found between hepatic sEH activity and plasma 14,15-EET levels following CHI. (*E–G*) The plasma levels of 14,15-EET in mice following genetic manipulation of hepatic sEH and their control animals (n = 6). (*H*) Negative correlation between hepatic sEH activity and plasma 14,15-EET levels following genetic manipulations of hepatic sEH after CCI. (*I*) The plasma and cortex levels of 14,15-EET-d_{11} 1 min after 14,15-EET-d_{11} injection in adult male C57BL/6J mice (n = 6). (*J*) The plasma and cortex levels of 14,15-EET-d_{11} 1 min after 14,15-EET-d_{11} injection in CCI mice (n = 7). (*K*) The cortex levels of 14,15-EET at 4 d post-CCI in WT and cKO mice (n = 9). Statistical significance was determined using the Brown–Forsythe and Welch ANOVA followed by the Dunnett's T3 post-hoc test for *A*, one-way ANOVA with the Dunnett's post-hoc test for *C*; the Pearson's correlation test for *B*, *D*, and *H*; or two-tailed unpaired Student's *t* test for *E–G* and *I–K*. Data are presented as the means ± SEM. Asterisks indicate significant differences (*P < 0.05, **P< 0.01, ***P < 0.001).

1-trifluoromethoxyphenyl-3-(1-propionylpiperidine-4-yl) urea (TPPU) (*SI Appendix*, Fig. S5*A*). We detected 14,15-EET-d_{11} in the plasma and cortex 1 min after injection. As a control, 14,15-EET-d_{11} was not detected in TPPU-treated mice after injection of artificial cerebrospinal fluid (ACSF) (Fig. 4*I* and *SI Appendix*, Fig. S5*B*). Moreover, in the CCI model, 14,15-EET-d_{11} was detected in the plasma and cortex 1 min after the 14,15-EET-d_{11} injection (Fig. 4*J*). These results clearly showed that 14,15-EET rapidly crossed the BBB. Intriguingly, we detected 14,15-DHET-d_{11} in the plasma and brain tissue 1 min after 14,15-EET-d_{11} injection. Notably, 14,15-EET-d_{11} was not detected 30 min after injection, although there remained a small amount of 14,15-DHET-d_{11} in the plasma (*SI Appendix*, Fig. S5). These results indicate that 14,15-EET can be rapidly degraded to 14,15-DHET. Indeed, we found that 14,15-EET levels were significantly increased in the cortex of cKO mice compared to those in WT mice 4 d after CCI (Fig. 4*K*), possibly due to BBB leakage. Taken together, these results suggest that increased plasma levels of 14,15-EET contribute to the neuroprotective role of the liver in TBI.

14,15-EET Application Produced Neuroprotective Effect in CCI Mouse Model. We investigated the effects of 14,15-EET on TBI. To this end, 14,15-EET (1 μg/2.5 μL) or ACSF was directly delivered onto the surface of the injured brain area starting at 30 min after CCI, and each behavioral test was conducted 30 min after 14,15-EET application (Fig. 5*A*). Compared to controls, mice treated with 14,15-EET exhibited significantly reduced ipsilateral brain edema and fewer TUNEL+ cells 24 h after CCI (Fig. 5 *B* and *C*). Moreover, 4-d treatment with 14,15-EET significantly reduced lesion volume and BBB permeability, as evidenced by decreased Evans blue extravasation and MMP-9 protein levels (Fig. 5 *D–F* and *SI Appendix*, Fig. S6 *A–C*). Moreover, 14,15-EET application significantly improved behavioral performance in the OFT, rotarod test, and Y-maze test following CCI compared to the controls (Fig. 5 *G–I*). These results indicated that 14,15-EET application produced neuroprotective effect in the CCI mouse model. In addition, we found that 14,15-EET application significantly decreased the covered area, number, soma volume, and mean intensity of GFAP+ astrocytes in the injured cortex; increased the expressions of *Bdnf*, *Tgf-β1*, *Igf-1*, and *Lif*; and promoted the generation of A2 phenotype astrocytes in the injured cortex of mice following CCI, indicating that 14,15-EET application mimicked the effect of hepatic sEH ablation at a biological level (Fig. 5 *J–M* and *SI Appendix*, Fig. S6*D*). Together, these results suggest that increased plasma levels of 14,15-EET mediate the neuroprotective effects of hepatic sEH ablation following CCI.

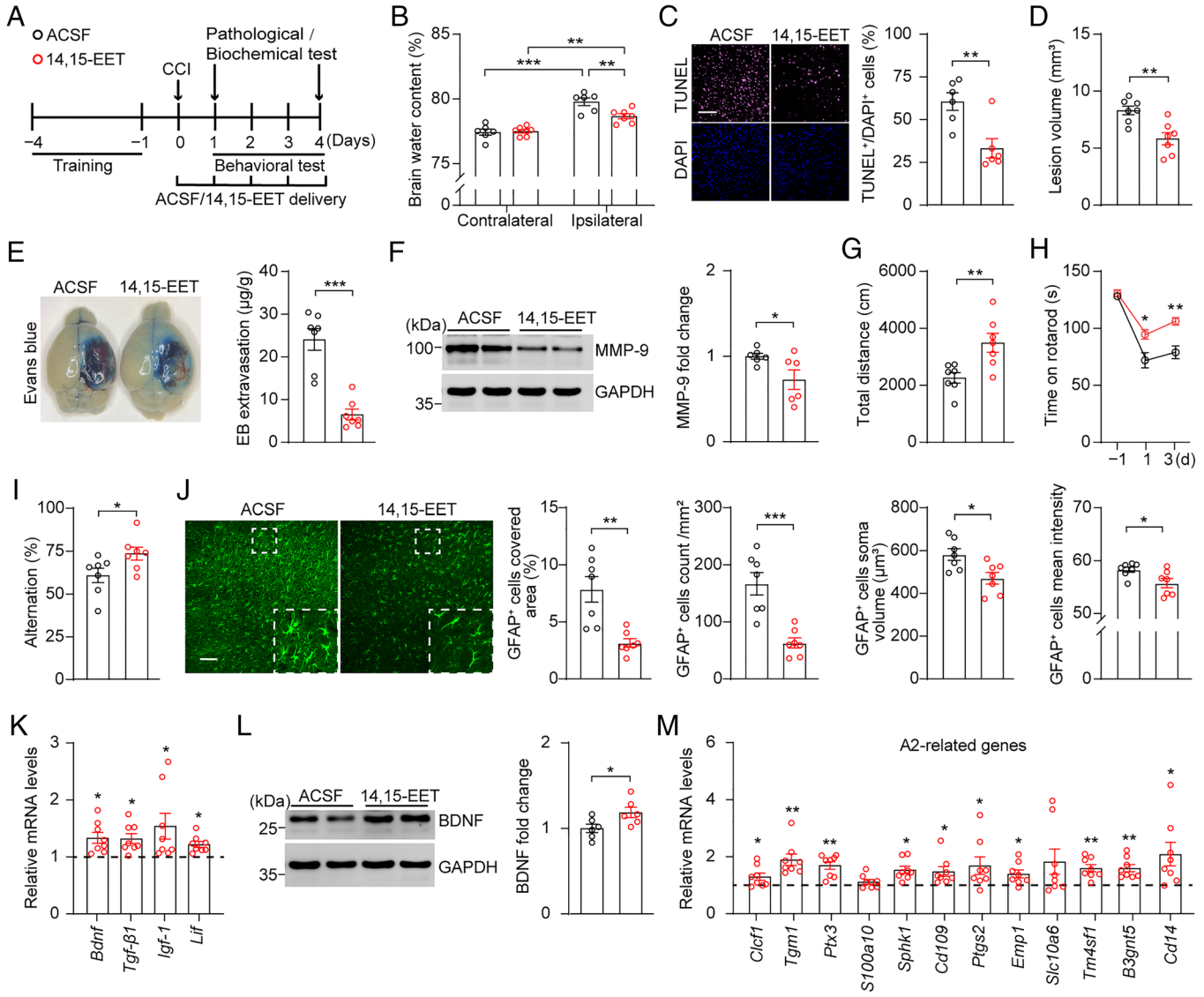

Fig. 5. 14,15-EET application produced neuroprotective effect in adult C57BL/6J mice following CCI. (*A*) Schematic diagram of the experimental design. Black circles, ACSF; red circles,14,15-EET. (*B*) The water content in the ipsilateral and contralateral cortices (ACSF, *n* = 6; 14,15-EET, *n* = 7). (*C*, *Left*) representative TUNEL (purple) and DAPI-stained (blue) brain slices of mice treated with ACSF or 14,15-EET 1 d post-CCI; (*C*, *Right*) quantification analysis percentage of TUNEL+/DAPI+ cells (*n* = 6). (Scale bar: 100 μm.) (*D*) Quantitative analysis of brain lesion volume (*n* = 7). (*E*) Quantitation of Evans blue extravasation in the brain at 4 d post-CCI (*n* = 7). (*F*) Western blotting and quantification of protein levels of MMP-9 in the injured cortex at 4 d post-CCI (*n* = 6). (*G–I*) Behavioral changes in the OFT (*G*), rotarod performance test (*H*), and Y-maze test (*I*) in adult C57BL/6J mice treated with ACSF or 14,15-EET following CCI (*n* = 7). (*J*) Representative images of GFAP+ astrocytes in the injured cortex; the proportion of covered area, number, soma volume, and mean intensity of GFAP+ astrocytes were quantitatively analyzed (*n* = 7). (Scale bar: 100 μm.) (*K*) Relative mRNA levels of neuroprotective factors in the injured cortex (dashed line indicates the mean levels of each corresponding gene in mice treated with ACSF, *n* = 8). (*L*) Western blotting and quantification of cortex BDNF at 4 d post-CCI (*n* = 6). (*M*) Relative mRNA levels of genes associated with A2 phenotype astrocytes in the injured cortex (dashed line indicates the mean levels of each corresponding gene in mice treated with ACSF, *n* = 8). Statistical significance was determined using two-way ANOVA followed by the Bonferroni's post-hoc test for *B*; two-tailed unpaired Student's *t* test for *C–G*, *I*, *J*, and *L*; two-way repeated-measures ANOVA followed by the Bonferroni's post-hoc test for *H*; or multiple *t* tests for *K* and *M*. Data are presented as the means ± SEM. Asterisks indicate significant differences (*$P < 0.05$, **$P < 0.01$, ***$P < 0.001$).

14,15-EEZE Application Attenuated the Neuroprotective Effect of Hepatic sEH Ablation in CCI. Finally, we investigated whether increased plasma levels of 14,15-EET are necessary for the neuroprotective effects of hepatic *Ephx2* deletion. To this end, we directly delivered 14,15-epoxyeicosa-5(Z)-enoic acid (14,15-EEZE; 1 μg/2.5 μL), an antagonist of 14,15-EET (41), or ACSF onto the surface of the injured brain area in both WT and cKO mice 30 min after CCI, and each behavioral test was conducted 30 min after 14,15-EEZE application (*SI Appendix*, Fig. S7*A*). We found that the smaller lesion volume induced by hepatic sEH ablation was blocked by 14,15-EEZE application, whereas 14,15-EEZE alone had little effect on the lesion volume following CCI (Fig. 6 *A* and *B* and *SI Appendix*, Fig. S7*B*). Moreover, the beneficial effects of hepatic sEH ablation on behavioral performance in the OFT, rotarod test, and Y-maze test were attenuated by 14,15-EEZE application (Fig. 6 *C–E*). Furthermore, the increased mRNA levels of *Bdnf*, *Tgf-β1* and *Igf-1* and genes related to A2 astrocytes induced by hepatic sEH ablation following CCI were completely blocked by 14,15-EEZE application (Fig. 6 *F* and *G*). Additionally, both hepatic sEH ablation and 14,15-EEZE application had little effect on the expression of genes related to A1 astrocytes (*SI Appendix*, Fig. S7*C*). These results strongly suggest that increased plasma levels of 14,15-EET mediate the neuroprotective effects of hepatic sEH ablation.

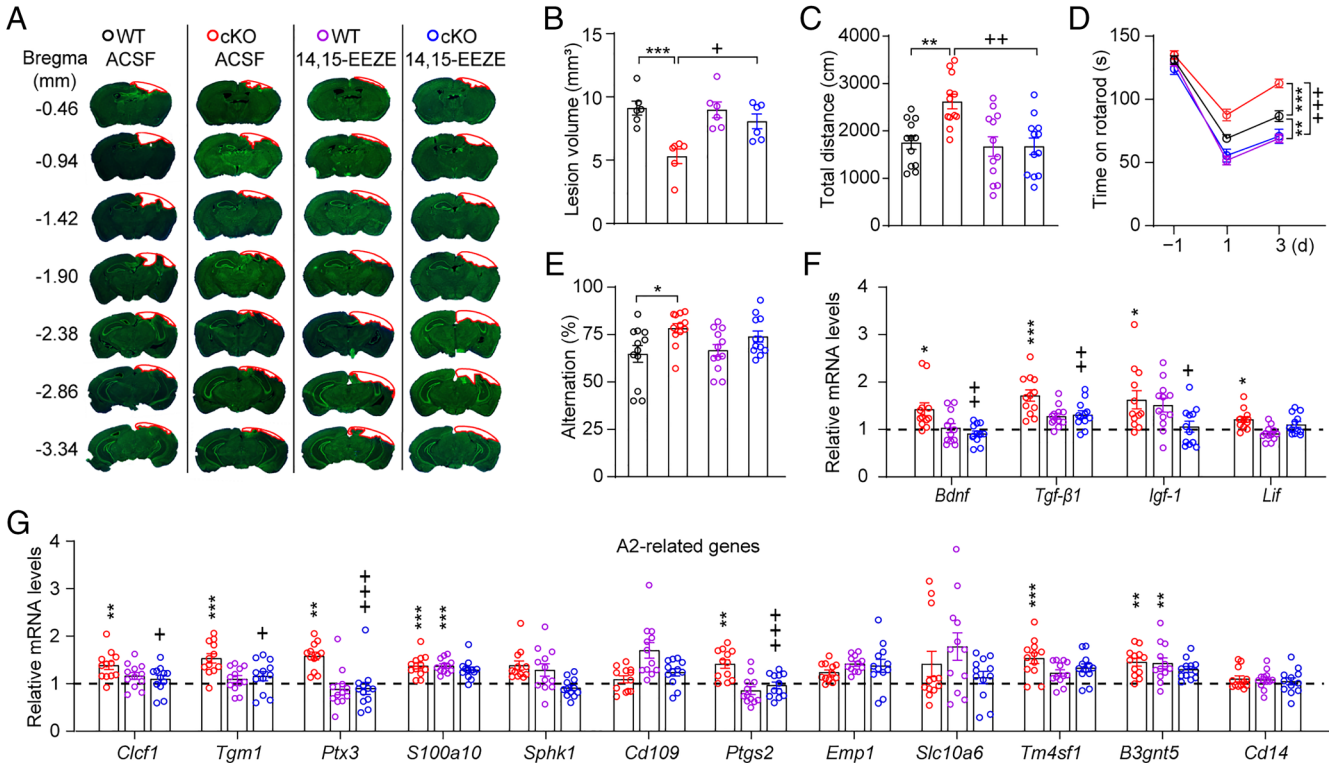

Fig. 6. 14,15-EEZE application abolished the neuroprotective effect of hepatic sEH ablation in the CCI mouse model. (*A*) Representative images of Nissl staining for WT and cKO mice treated with ACSF or 14,15-EEZE. The red outline shows the loss area of injured brain. (*B*) Quantitative analysis of brain lesion volume ($n = 6$). (*C*–*E*) Behavioral changes in the OFT (*C*), rotarod performance test (*D*), and Y-maze test (*E*) in WT and cKO mice treated with ACSF or 14,15-EEZE ($n = 12$). (*F*) The increased mRNA levels of neuroprotective factors in the injured cortex induced by hepatic sEH ablation were blocked by 14,15-EEZE (dashed line indicates the mean levels of each corresponding gene in WT controls treated with ACSF, $n = 12$). (*G*) Relative mRNA levels of genes associated with A2 phenotype astrocytes in the injured cortex (dashed line indicates the mean levels of each corresponding gene in WT controls treated with ACSF, $n = 12$). Statistical significance was determined using two-way ANOVA followed by the Bonferroni's post-hoc test for *B*, *C*, and *E*–*G*; or two-way repeated-measures ANOVA followed by the Bonferroni's post-hoc test for *D*. Data are presented as the means ± SEM. Asterisks or plus signs indicate significant differences (*$P < 0.05$, **$P < 0.01$, ***$P < 0.001$ vs. ACSF-treated WT mice; $^{+}P < 0.05$, $^{++}P < 0.01$, $^{+++}P < 0.001$ vs. ACSF-treated cKO mice).

Discussion

In the present study, we provide evidence that the liver plays a key role in the pathology of TBI. The major outcomes of this study were as follows: First, we found that the enzymatic activity of hepatic sEH was specifically altered in two mouse models of TBI, CCI, and CHI. Second, genetic deletion or knockdown of hepatic sEH rescued the CCI-induced pathology and improved the recovery of neurological functions. In contrast, overexpression of *Ephx2* in the liver exacerbated CCI-associated neurological impairments. Third, the knockout of hepatic *Ephx2* promoted the generation of A2 phenotype astrocytes in the injured cortex and promoted the production of astrocyte-associated neuroprotective factors following CCI. Fourth, increased plasma 14,15-EET levels mediated the neuroprotective effects of hepatic sEH ablation. These results highlight the role of the liver in the pathophysiology of TBI and strongly suggest that enhancing the neuroprotective role of the liver could be a unique avenue for developing therapeutic treatments for TBI.

Our study has particularly high translational potential. Previous studies have shown that 14,15-EET exerts a variety of beneficial effects on the pathology and treatment of central nervous system disorders, such as stroke, Parkinson's disease, epilepsy, cognitive impairment, dementia, and depression (42). In the present study, we found that the direct delivery of 14,15-EET to the surface of the injured brain rescued CCI-induced pathology and ameliorated the associated neurological deficits. This indicates that 14,15-EET has the potential for development as a neuroprotective drug, especially as an external medicine. In addition, gene therapy has recently become a hot topic for its potential to treat TBI; however, obstacles, such as low permeability through the BBB, significantly limit its therapeutic potential (43), highlighting the need for the development of a suitable AAV-based delivery system to treat central nervous system diseases. Gene therapy via peripheral intravenous administration can achieve high levels of gene transfer into hepatocytes in mammals, including humans, with few extrahepatic effects (44). Owing to its unique anatomical properties, the liver is the preferred target for AAV-based gene therapy (45). In our study, downregulation of hepatic *Ephx2 via* tail vein injection of rAAV2/8-eGFP-*Ephx2*-shRNA ameliorated neurological deficits and improved neurological function recovery. Moreover, our previous study showed that hepatic sEH ablation had little effect on body weight, blood pressure, or plasma glucose levels (9). These results strongly suggest that targeting hepatic EET signaling is a realistic therapeutic option for treating TBI.

Previous studies have found differences in the core expression genes and functions of reactive astrocytes stimulated by LPS or stroke, known as A1 and A2 phenotype astrocytes, respectively; A1 is harmful, while A2 has neuroprotective effects (37). Studies have shown that astrocytes are significantly activated, and the numbers of A1 astrocytes increased following TBI (46, 47). In the present study, we found that hepatic sEH ablation had little effect on the mRNA levels of genes related to A1 following CCI.

However, *Lif* mRNA levels were significantly increased in the injured cortex of cKO mice and 14,15-EET-treated mice following CCI compared to the respective control animals. Because Lif was only increased in stroke-induced astrocytes, but not in LPS-induced astrocytes (38), this result indicated that hepatic sEH ablation promoted the generation of A2 phenotype astrocytes following TBI. Indeed, we found that both 14,15-EET treatment and hepatic sEH ablation significantly increased the expression of astrocyte-related neuroprotective factors, including BDNF, TGF-β1, and IGF-1. Taken together, these results suggest that generation of A2 astrocytes may be involved in the liver's neuroprotection following TBI. Future studies are needed to understand the mechanisms by which hepatic sEH activity regulates A2 astrocyte generation following TBI and the broad role of the A2:A1 ratio in the pathology across multiple forms of neurodegeneration.

In addition, we found that hepatic sEH activity transiently and rapidly decreased after TBI. However, no changes were observed in the protein or mRNA levels of sEH in the liver in the time window following TBI. These results indicate that a signal originating from the injured brain area may be involved in the regulation of the liver–brain axis. Future studies are needed to illustrate the mechanism underlying the regulation of sEH activity, which would be presumed to provide therapeutic benefits.

Materials and Methods

Details of the experimental protocols, including *Materials*, *Animals*, *TBI Model*, *Adeno-associated Viruses*, *Behavioral Test*, *Immunohistochemistry*, *Evans Blue Extravasation Assays*, *Western Blotting*, *qRT-PCR*, *LC–MS/MS Analysis for EETs and DHETs*, and *Statistical Analysis*, are given in *SI Appendix, Materials and Methods*.

Data, Materials, and Software Availability. All study data are included in the article and/or supporting information.

ACKNOWLEDGMENTS. We would like to thank M.S. Xue-Fang Zeng and Shengquan Zheng, Pazhou Lab, for their technical supports. This work was supported by the National Natural Science Foundation of China (81930034 to X.Z.) and Scientific and Technological Innovation 2030 of China–Major projects (2022ZD0211700 to X.Z.). Partial support was provided by NIH–National Institute of Environmental Health Sciences (RIVER Award) R35 ES030443-01 and NIH-National Institute of Neurological Disorders and Stroke U54 NS127758 (Counter Act Program).

Author affiliations: [a]School of Basic Medical Science, Southern Medical University, Guangzhou 510515, China; [b]Research Center for Brain Health, Pazhou Lab, Guangzhou 510330, China; [c]School of Psychology, Shenzhen University, Shenzhen 518060, China; [d]Department of Entomology and Nematology, University of California, Davis, CA 95616; [e]University of California Davis Comprehensive Cancer Center, University of California, Davis, CA 95616; and [f]School of Biology and Biological Engineering, South China University of Technology, Guangzhou 510006, China

Author contributions: B.D.H., and X.Z. designed research; Y.D., J.D., Y.W., M.Z., W.X., H.L., and Y.Z. performed research; Y.W. and M.Z. contributed new reagents/analytic tools; Y.D., J.D., and X.Z. analyzed data; and Y.D., J.D., B.D.H., and X.Z. wrote the paper.

1. A. I. R. Maas *et al.*, Traumatic brain injury: Integrated approaches to improve prevention, clinical care, and research. *Lancet Neurol.* **16**, 987–1048 (2017).
2. T. Janowitz, D. K. Menon, Exploring new routes for neuroprotective drug development in traumatic brain injury. *Sci. Trans. Med.* **2**, 27rv21 (2010).
3. W. Qu *et al.*, Disrupting nNOS-PSD95 interaction improves neurological and cognitive recoveries after traumatic brain injury. *Cereb. Cortex* **30**, 3859–3871 (2020).
4. M. Du *et al.*, A novel circular RNA, circIgfbp2, links neural plasticity and anxiety through targeting mitochondrial dysfunction and oxidative stress-induced synapse dysfunction after traumatic brain injury. *Mol. Psychiatry* **27**, 4575–4589 (2022).
5. R. Vink, A. J. Nimmo, Multifunctional drugs for head injury. *Neurotherapeutics* **6**, 28–42 (2009).
6. S. J. McDonald *et al.*, Beyond the brain: Peripheral interactions after traumatic brain injury. *J. Neurotrauma* **37**, 770–781 (2020).
7. M. R. Somayaji, A. J. Przekwas, R. K. Gupta, Combination therapy for multi-target manipulation of secondary brain injury mechanisms. *Curr. Neuropharmacol.* **16**, 484–504 (2018).
8. M. Arnoriaga-Rodriguez *et al.*, Obesity impairs short-term and working memory through gut microbial metabolism of aromatic amino acids. *Cell Metab.* **32**, 548–560 e547 (2020).
9. X. H. Qin *et al.*, Liver soluble epoxide hydrolase regulates behavioral and cellular effects of chronic stress. *Cell Rep.* **29**, 3223–3234 e3226 (2019).
10. N. A. Kerr *et al.*, Traumatic brain injury-induced acute lung injury: Evidence for activation and inhibition of a neural-respiratory-inflammasome axis. *J. Neurotrauma* **35**, 2067–2076 (2018).
11. T. J. Treangen, J. Wagner, M. P. Burns, S. Villapol, Traumatic brain injury in mice induces acute bacterial dysbiosis within the fecal microbiome. *Front. Immunol.* **9**, 2757 (2018).
12. S. Y. Cheon, J. Song, The association between hepatic encephalopathy and diabetic encephalopathy: The brain-liver axis. *Int. J. Mol. Sci.* **22**, 463 (2021).
13. C. C. Chen, Y. C. Huang, C. N. Yeh, Neurosurgical procedures in patients with liver cirrhosis: A review. *World J. Hepatol.* **7**, 2352–2357 (2015).
14. R. Prus *et al.*, A histological and morphometric assessment of the adult and Juvenile rat livers after mild traumatic brain injury. *Cells* **10**, 1121 (2021).
15. J. D. Lecques *et al.*, N-3 polyunsaturated fatty acids ameliorate neurobehavioral outcomes post-mild traumatic brain injury in the fat-1 mouse model. *Nutrients* **13**, 4092 (2021).
16. R. P. Bazinet, S. Laye, Polyunsaturated fatty acids and their metabolites in brain function and disease. *Nat. Rev. Neurosci.* **15**, 771–785 (2014).
17. W. Chen *et al.*, 14,15-Epoxyeicosatrienoic acid alleviates pathology in a mouse model of Alzheimer's disease. *J. Neurosci.* **40**, 8188–8203 (2020).
18. W. Xiong *et al.*, Astrocytic epoxyeicosatrienoic acid signaling in the medial prefrontal cortex modulates depressive-like behaviors. *J. Neurosci.* **39**, 4606–4623 (2019).
19. K. I. Strauss, A. Gruzdev, D. C. Zeldin, Altered behavioral phenotypes in soluble epoxide hydrolase knockout mice: Effects of traumatic brain injury. *Prostaglandins Other Lipid Mediat.* **104–105**, 18–24 (2013).
20. L. Yuan *et al.*, 14,15-epoxyeicosatrienoic acid promotes production of brain derived neurotrophic factor from astrocytes and exerts neuroprotective effects during ischaemic injury. *Neuropathol. Appl. Neurobiol.* **42**, 607–620 (2016).
21. T. H. Hung *et al.*, Deletion or inhibition of soluble epoxide hydrolase protects against brain damage and reduces microglia-mediated neuroinflammation in traumatic brain injury. *Oncotarget* **8**, 103236–103260 (2017).
22. D. Xu *et al.*, Prevention and reversal of cardiac hypertrophy by soluble epoxide hydrolase inhibitors. *Proc. Natl. Acad. Sci. U.S.A.* **103**, 18733–18738 (2006).
23. Y. Wu *et al.*, Mild traumatic brain injury induces microvascular injury and accelerates Alzheimer-like pathogenesis in mice. *Acta Neuropatholog. Commun.* **9**, 74 (2021).
24. M. A. Flierl *et al.*, Mouse closed head injury model induced by a weight-drop device. *Nat. Protocols* **4**, 1328–1337 (2009).
25. S. Liu *et al.*, Induction of neuronal PI3Kgamma contributes to endoplasmic reticulum stress and long-term functional impairment in a murine model of traumatic brain injury. *Neurotherapeutics* **16**, 1320–1334 (2019).
26. S. E. Gruenbaum, A. Zlotnik, B. F. Gruenbaum, D. Hersey, F. Bilotta, Pharmacologic neuroprotection for functional outcomes after traumatic brain injury: A systematic review of the clinical literature. *CNS Drugs* **30**, 791–806 (2016).
27. F. Alqahtani *et al.*, Coadministration of ketamine and perampanel improves behavioral function and reduces inflammation in acute traumatic brain injury mouse model. *BioMed. Res. Int.* **2020**, 3193725 (2020).
28. D. J. Vita, C. J. Meier, K. Broadie, Neuronal fragile X mental retardation protein activates glial insulin receptor mediated PDF-Tri neuron developmental clearance. *Nat. Commun.* **12**, 1160 (2021).
29. M. W. Ma *et al.*, NADPH oxidase in brain injury and neurodegenerative disorders. *Mol. Neurodegener.* **12**, 7 (2017).
30. J. Wu *et al.*, Soluble epoxide hydrolase inhibitor protects against blood-brain barrier dysfunction in a mouse model of type 2 diabetes via the AMPK/HO-1 pathway. *Biochem. Biophys. Res. Commun.* **524**, 354–359 (2020).
31. X. Yi *et al.*, 1-Trifluoromethoxyphenyl-3-(1-Propionylpiperidin-4-yl) Urea protects the blood-brain barrier against ischemic injury by upregulating tight junction protein expression, mitigating apoptosis and inflammation in vivo and in vitro model. *Front. Pharmacol.* **11**, 1197 (2020).
32. Y. Tian *et al.*, Soluble epoxide hydrolase inhibitor attenuates BBB disruption and neuroinflammation after intracerebral hemorrhage in mice. *Neurochem. Int.* **150**, 105197 (2021).
33. T. Carlson, M. Kroenke, P. Rao, T. E. Lane, B. Segal, The Th17-ELR+ CXC chemokine pathway is essential for the development of central nervous system autoimmune disease *J. Exp. Med.* **205**, 811–823 (2008).
34. T. Liu, T. Zhang, H. Yu, H. Shen, W. Xia, Adjudin protects against cerebral ischemia reperfusion injury by inhibition of neuroinflammation and blood-brain barrier disruption. *J. Neuroinflammation* **11**, 107 (2014).
35. E. Csuka *et al.*, Cell activation and inflammatory response following traumatic axonal injury in the rat. *Neuroreport* **11**, 2587–2590 (2000).
36. D. J. Myer, G. G. Gurkoff, S. M. Lee, D. A. Hovda, M. V. Sofroniew, Essential protective roles of reactive astrocytes in traumatic brain injury. *Brain J. Neurol.* **129**, 2761–2772 (2006).
37. J. L. Zamanian *et al.*, Genomic analysis of reactive astrogliosis. *J. Neurosci.* **32**, 6391–6410 (2012).
38. S. Bauer, B. J. Kerr, P. H. Patterson, The neuropoietic cytokine family in development, plasticity, disease and injury. *Nat. Rev. Neurosci.* **8**, 221–232 (2007).
39. C. Morisseau, B. D. Hammock, Impact of soluble epoxide hydrolase and epoxyeicosanoids on human health. *Ann. Rev. Pharmacol. Toxicol.* **53**, 37–58 (2013).
40. T. R. Harris, B. D. Hammock, Soluble epoxide hydrolase: Gene structure, expression and deletion. *Gene* **526**, 61–74 (2013).
41. K. M. Gauthier *et al.*, 14,15-Epoxyeicosa-5(Z)-enoic acid: A selective epoxyeicosatrienoic acid antagonist that inhibits endothelium-dependent hyperpolarization and relaxation in coronary arteries. *Circulation Res.* **90**, 1028–1036 (2002).
42. S. Zarriello *et al.*, Humble beginnings with big goals: Small molecule soluble epoxide hydrolase inhibitors for treating CNS disorders. *Progress Neurobiol.* **172**, 23–39 (2019).
43. F. Shen, L. Wen, X. Yang, W. Liu, The potential application of gene therapy in the treatment of traumatic brain injury. *Neurosurg. Rev.* **30**, 291–298 (2007).
44. L. M. Kattenhorn *et al.*, Adeno-associated virus gene therapy for liver disease. *Hum. Gene Therapy* **27**, 947–961 (2016).
45. F. Mingozzi, K. A. High, Therapeutic in vivo gene transfer for genetic disease using AAV: Progress and challenges. *Nat. Rev. Genet.* **12**, 341–355 (2011).
46. J. Xing *et al.*, Single-cell RNA sequencing reveals cellular and transcriptional changes associated with traumatic brain injury. *Front. Genet.* **13**, 861428 (2022).
47. D. P. Q. Clark *et al.*, Inflammation in traumatic brain injury: Roles for toxic A1 astrocytes and microglial-astrocytic crosstalk. *Neurochem. Res.* **44**, 1410–1424 (2019).